NEUROSCIENCE

Encoding of environmental illumination by primate melanopsin neurons

Andreas Liu[1]**, Elliott S. Milner[1]†**, Yi-Rong Peng[2]‡, Hannah A. Blume[1], Michael C. Brown[1], Gregory S. Bryman[1]§, Alan J. Emanuel[1]#, Philippe Morquette[1], Nguyen-Minh Viet[1], Joshua R. Sanes[2], Paul D. Gamlin[3], Michael Tri H. Do[1]*

Light regulates physiology, mood, and behavior through signals sent to the brain by intrinsically photosensitive retinal ganglion cells (ipRGCs). How primate ipRGCs sense light is unclear, as they are rare and challenging to target for electrophysiological recording. We developed a method of acute identification within the live, ex vivo retina. Using it, we found that ipRGCs of the macaque monkey are highly specialized to encode irradiance (the overall intensity of illumination) by blurring spatial, temporal, and chromatic features of the visual scene. We describe mechanisms at the molecular, cellular, and population scales that support irradiance encoding across orders-of-magnitude changes in light intensity. These mechanisms are conserved quantitatively across the ~70 million years of evolution that separate macaques from mice.

Many visual functions are non–image-forming: they respond less to details in the scene than to irradiance. For example, irradiance indicates the Sun's position in the sky and is therefore used to synchronize the circadian clock with local time, regulating patterns of physiology and gene expression in practically every tissue (*1*). IpRGCs are necessary for circadian photoregulation and many other non-image visual functions (*2*). These neurons sense light directly using a G protein–coupled receptor called melanopsin and indirectly through retinal circuitry (*2*, *3*). We investigated how primate ipRGCs encode irradiance, focusing on two key requirements: insensitivity to image detail and the signaling of light levels spanning several orders of magnitude from night to day (*1*, *4*). Our study rests on two technical advances: First, we developed an immunotagging-based approach that identifies these rare neurons acutely in the live, ex vivo retina, making them accessible to single cell analysis. Second, we transplanted macaque melanopsin into mouse ipRGCs, allowing properties of this molecule to be examined in a well-defined context. Our experiments concern the intrinsic, melanopsin-driven light response that distinguishes ipRGCs from other retinal output neurons (*2*, *5*).

[1]F. M. Kirby Neurobiology Center and Department of Neurology, Boston Children's Hospital and Harvard Medical School. Boston, MA 02115, USA. [2]Department of Molecular and Cellular Biology and Center for Brain Science, Harvard University, Cambridge, MA 02138, USA. [3]Department of Ophthalmology and Visual Sciences, University of Alabama at Birmingham, Birmingham, AL, 35294, USA.
*Corresponding author. Email: michael.do@childrens.harvard.edu
†Present address: Sainsbury Wellcome Centre for Neural Circuits and Behavior, University College London, London, W1T 4JG, UK.
‡Present address: Department of Ophthalmology, Stein Eye Institute, UCLA David Geffen School of Medicine, Los Angeles, CA 90095, USA.
§Present address: Merck & Co., Inc., Cambridge, MA 02141, USA.
#Present address: Department of Cell Biology, Emory University School of Medicine, Atlanta, GA, 30322, USA.
**These authors contributed equally to this work.

Ex vivo, live identification of macaque ipRGCs

In humans and other primates, ipRGCs constitute ~0.4% of the retinal output neurons (*6*) and require a reliable method of identification for systematic study. To examine their electrical responses, live identification is needed (*3*, *7*). We sought an ex vivo method that could be applied acutely to live tissue collected opportunistically. We raised an antibody against melanopsin's N terminus. The antibody labeled live cells with the morphological features of ipRGCs (*3*, *6*) (Fig. 1, A and B). We further validated the antibody using heterologous expression of macaque melanopsin in cell lines and mouse ipRGCs (Fig. 2 and figs. S1 and S2). We compared light responses between macaque ipRGCs (identified with antibody) and mouse ipRGCs expressing macaque melanopsin in place of their own (identified without antibody) and detected no differences in melanopsin function (see below). This method of identifying cells within live tissue should generalize to other cell types of any species for which ectodomain markers are accessible.

Our study concerns outer-stratifying ipRGCs, whose dendrites are placed deep within the retina (henceforth, simply "ipRGCs"; see Methods). They are anatomical orthologs of the M1 type of rodent ipRGCs. M1 ipRGCs have the highest melanopsin expression, exhibit the largest intrinsic light responses, and are essential drivers of non-image visual functions that include circadian photoregulation (*2*, *8*, *9*). To focus on cell-autonomous mechanisms, we applied antagonists of synaptic transmission in all electrophysiological experiments.

Macaque melanopsin supports temporal and spatial integration

To study how macaque ipRGCs encode irradiance, we examined the electrical spikes that they fire to convey visual information to the brain. Even when driven by their intrinsic responses alone, ipRGCs spiked during illumination and long afterward; post-illumination, persistent firing lasted 270 ± 50 s (mean ± SD, 3 cells examined at 35°C; Fig. 1C). Macaques make large eye movements several times per second to scan a given visual scene (*10*). Persistent spiking continues over more than a thousand such saccades, blurring spatial information and favoring irradiance encoding.

We asked how persistent spiking is driven by melanopsin, a pigment of the rhabdomeric type (*2*). These pigments tend to be bistable: when the ground state absorbs a photon, it switches to an active state that has a long lifetime (*11*). When the active state absorbs a photon, it switches to the ground state, deactivating the cell. Evidence for bistability has been reported for the melanopsin of primates (*12*) and the invertebrate amphioxus (*13*). These studies suggest that long-wavelength light (≥ ~560 nm) is preferentially absorbed by melanopsin's active state and should therefore produce deactivation, although this has not been tested directly in primate ipRGCs. We found that long-wavelength illumination acutely suppressed the persistent spiking of macaque ipRGCs (Fig. 1D and fig. S3; 3 of 3 cells). Thus, persistent spiking appears to originate with the long-lived active state of a photoswitchable melanopsin.

Because persistent activity can be mediated by voltage-gated ion channels (*14*), we clamped the membrane voltage to suppress these channels. Photoswitchable persistent responses remained (Fig. 1, E and F; 3 of 3 cells, decay time constant 123 to 404 s at 23°C), providing additional evidence that they arise from melanopsin.

Unlike the monostable pigments of rods and cones, which disassemble after activation and require accessory cells for reassembly (*2*), a melanopsin molecule that has been switched off by light is available immediately to be switched on again. This supports a sustained representation of irradiance. Indeed, without melanopsin some non-image visual functions are abnormally transient (*2*).

Macaque melanopsin supports a degree of wavelength integration

Our experiments indicate that melanopsin can be switched from an active to an electrically silent state but have not addressed the nature of that silent state. If melanopsin is bistable, that state is the ground state. However, mouse melanopsin appears tristable, possessing a ground state, an active state, and an "extra" state (E) that is electrically silent (*15*, *16*). The ground and active states absorb long wavelengths more effectively than the E state, so that long-wavelength light causes the E state to accumulate. We asked whether macaque melanopsin deactivates by returning to the ground state (consistent with bistability)

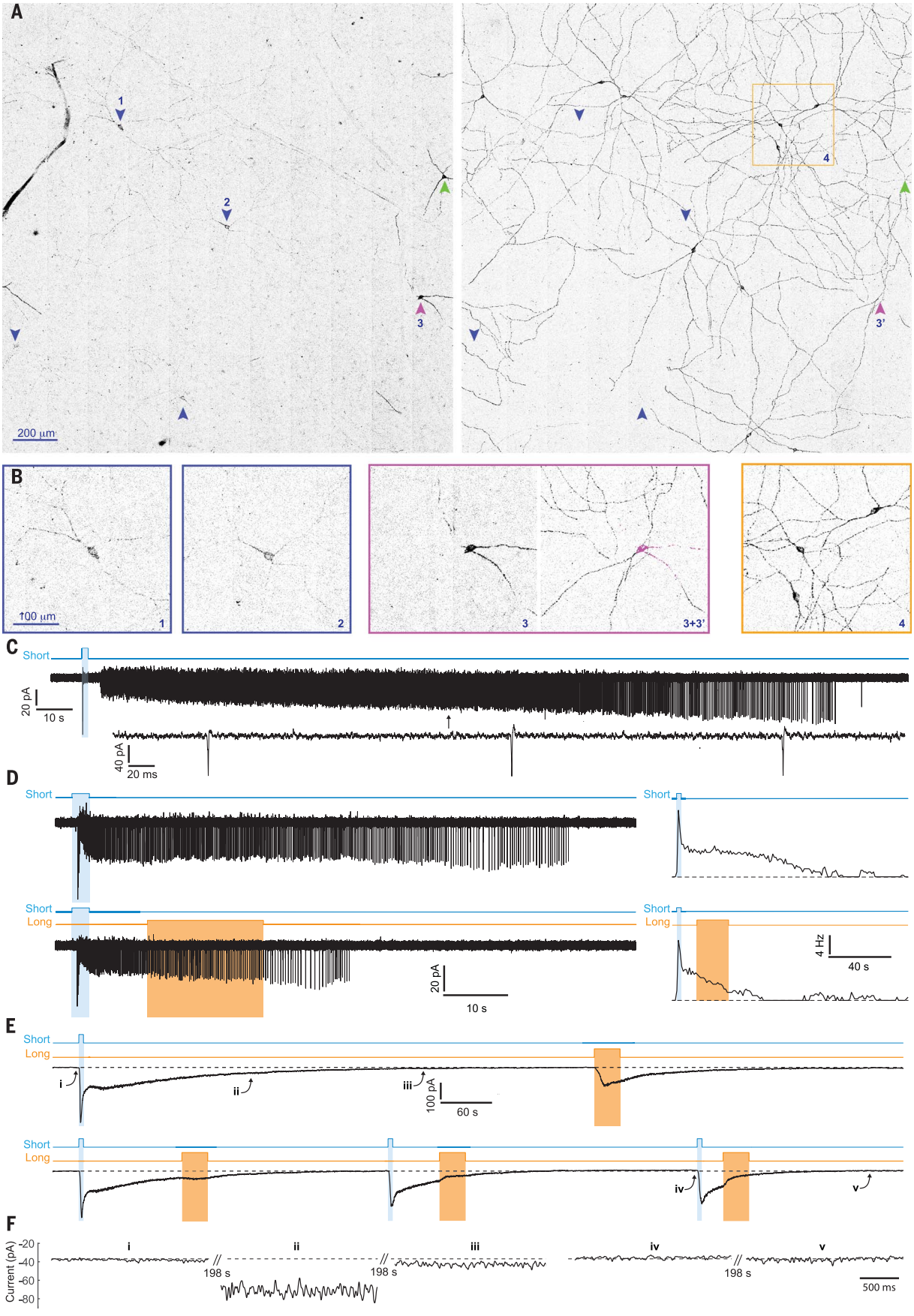

Figure 1

Fig. 1. Photoswitchable persistent responses in live-immunotagged macaque ipRGCs. (**A**) Antibody labeling in live tissue reveals diverse ipRGCs (inverted fluorescence images). (Left) Z projection through a 13.5-μm thick volume containing the ganglion cell layer (GCL) and inner aspect of the inner plexiform layer (IPL). Arrowheads mark ipRGCs with somata in the GCL. Fluorescence in the upper left is from a blood vessel. (Right) for the same XY position, a Z projection through a 29-μm thick volume containing the rest of the IPL and the inner aspect of the inner nuclear layer (INL). Arrowheads are in the same positions. (**B**) (Left to right) expanded views of two lightly stained ipRGCs with somata in the GCL; an outer-stratifying ipRGC with its soma in the GCL (superficial and deep projections juxtaposed); and three outer-stratifying ipRGCs with somata displaced to the INL [corresponding to the orange box in (A)]. (**C**) Loose patch recording. A pulse of short-wavelength light evokes persistent spiking near body temperature (35°C). The inset shows spike waveforms on an expanded time base (excerpt position marked with an arrow) (**D**) (Top) Persistent spiking in another ipRGC. Peristimulus time histogram (PSTH) for three trials shown on right (23°C). (Bottom) For the same cell, chasing the short-wavelength light with long-wavelength light curtails the persistent response (PSTH from three trials). (**E**) Perforated-patch recording in voltage clamp (−80 mV, 23°C). Short- and long-wavelength switching of persistent photocurrent. Long-wavelength light evokes current because some photon absorptions cycle melanopsin molecules through the signaling state, even as the photoequilibrium favors low occupancy of this state. Response traces are low-pass filtered at 2 Hz. (**F**) 2-s long segments of the same recording, keyed to time points in (E). Traces are low-pass filtered at 20 Hz. Synaptic antagonists. (For all figures, see Methods for stimulus details.)

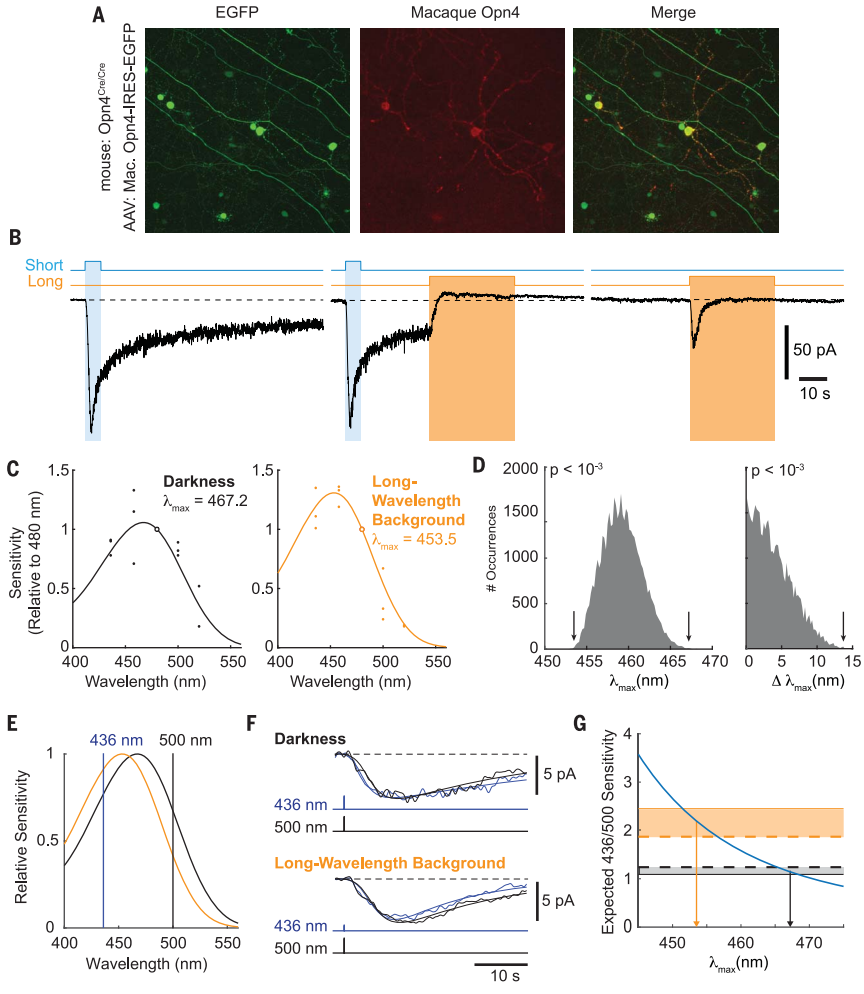

Fig. 2. Macaque melanopsin multistability underlies temporal and chromatic integration. (**A**) "Hybrid" mouse ipRGCs have both melanopsin alleles replaced by Cre recombinase (*Opn4*$^{Cre/Cre}$) and are transduced with a virus driving Cre-dependent macaque melanopsin and EGFP. Immunolabeling for EGFP and macaque melanopsin are shown with a merge. (**B**) Short- and long-wavelength switching of persistent phototransduction in a hybrid ipRGC. (**C**) Criterion action spectra measured in hybrid ipRGCs (Methods), reflecting the absorption spectra of macaque melanopsin, following prolonged darkness (left; 11 cells) or from atop a background of 600-nm light (right; 11 different cells). The data are fit to templates (*18*) for single pigment states, yielding peak wavelength sensitivity (λ_{max}) values of 467.2 nm (darkness) and 453.5 nm (600-nm background). Each curve is fit to two cells tested at 520 nm and three cells tested at each of three wavelengths: 436, 458, and 500 nm. Sensitivities at these wavelengths are normalized to the sensitivity at 480 nm (open circles). (**D**) (Left) Permutation test giving probabilities of observing λ_{max} >467.2 nm or <453.5 of 3.96×10^{-4} and 3.54×10^{-4}, respectively. (Right) Permutation test showing a small probability ($P = 5.00 \times 10^{-4}$) of observing a spectral separation between the two states of >13.7 nm by chance. Arrows indicate actual best-fit values. (**E**) Expected sensitivity to 436- and 500-nm light in darkness (ratio of 1.14) or atop a 600-nm background (ratio of 2.20) given the melanopsin states defined in (C). (**F**) Criterion responses evoked from a macaque ipRGC by 436- and 500-nm flashes under these adaptation conditions. Responses are fit using an equation with a sigmoidal rise and an exponential decay (Methods). Heights of flash monitors indicate relative stimulus intensity (photon density) at the two wavelengths. (**G**) A pigment state with a given λ_{max} (x axis) has an expected 436/500-nm sensitivity ratio (y axis) that is denoted by the blue curve. The λ_{max} values exhibited by hybrid ipRGCs under dark adaptation and 600-nm adaptation are indicated by black and orange vertical arrows, respectively. The 436/500-nm sensitivity ratios measured for two macaque ipRGCs under dark or 600-nm adaptation are shown as black and orange horizontal lines, respectively [the solid line represents the cell in (F) and the dashed line another cell; measurement ranges are shaded]. Synaptic antagonists, 23°C.

or by switching to another electrically silent state.

We examined macaque melanopsin in mouse ipRGCs that lacked their endogenous melanopsin alleles through replacement with Cre recombinase (*17*). These "hybrid" ipRGCs (mouse ipRGCs expressing macaque melanopsin) are relatively plentiful and provide a more physiological setting than immortalized cell lines and biochemical preparations (Fig. 2A and fig. S2). We recorded hybrid ipRGCs that are likely of the M1 type (*2*) (see Methods). Macaque melanopsin activates phototransduction in these neurons. Similar to macaque ipRGCs, hybrid ipRGCs produced persistent responses that were suppressed by long-wavelength light (Fig. 2B and fig. S4, A to C; 12 of 12 cells). We therefore used hybrid cells to study the electrically silent state induced by long-wavelength illumination.

We measured the wavelength sensitivity of cellular photoactivation (*11*, *15*, *18*). If macaque melanopsin were bistable, the action spectrum should be constant because it always reflects the absorption spectrum of the single ground state. However, this was not the case (Fig. 2C and fig. S4D). Following prolonged darkness

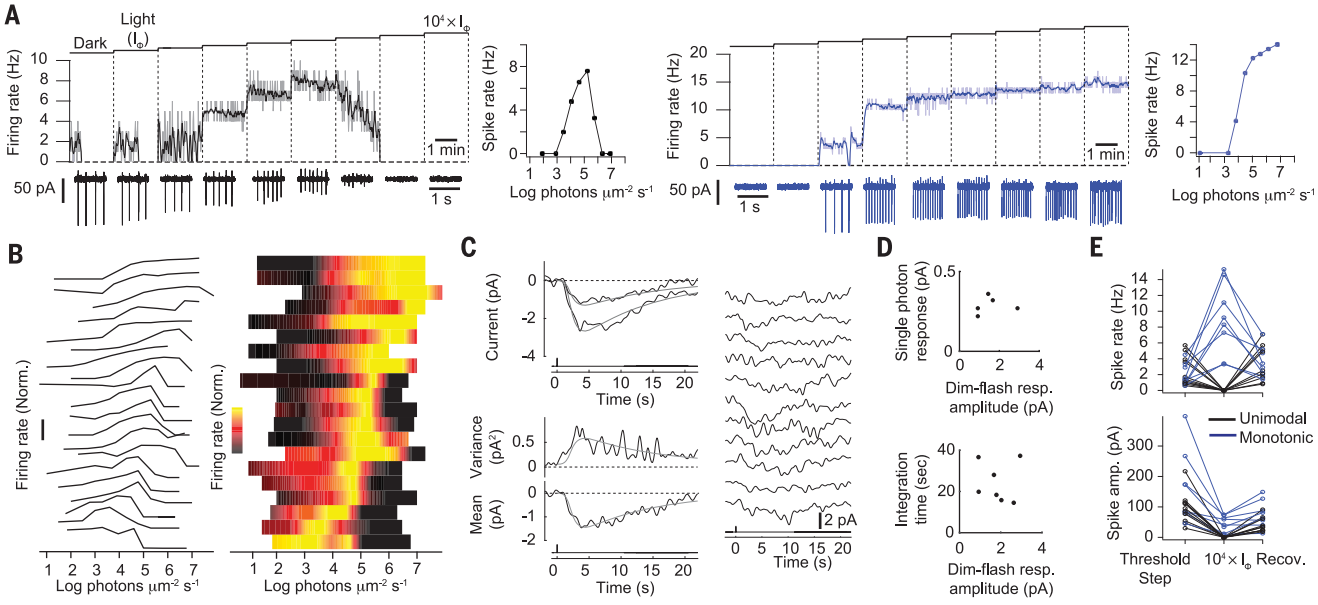

Fig. 3. Macaque ipRGCs collectively encode a broad range of light intensities through differential intrinsic tuning. (**A**) Loose-patch recordings from macaque ipRGCs. (Left) As light intensity increased, this cell increased spiking and then silenced. Its tuning curve (intensity-firing relation) is unimodal (right). Spikes diminished in size until silencing. Spiking resumed when light intensity decreased (fig. S6A). (Right) This cell increased spiking toward a plateau and did not silence. Its tuning curve is monotonic. (**B**) Unimodal and monotonic ipRGCs are tuned to different irradiances. Curves are normalized by their peaks and vertically offset for display. (**C**) Single photon response estimated using perforated-patch, voltage-clamp recordings (−80 mV) from macaque ipRGCs. (Upper left) Linear superposition of dim-flash responses in an ipRGC. When scaled by stimulus intensity, the same smooth curve (see Methods) fits both responses. Traces are averages of 16 trials, low-pass filtered at 0.5 Hz. (Lower left) Variance and mean of the same ipRGC's responses to 11 identical dim flashes (trials shown at right). The variance and the mean can be fit by the same smooth curve, scaled differently. Dividing the variance by the mean gives the estimated single photon response amplitude, which is 0.36 pA for this example. (Right) Individual trials for this cell. (**D**) The single photon response amplitude (variance/mean ratio) and the integration time (integral/peak ratio) computed in 5 and 7 ipRGCs, respectively. These parameters did not depend on the amplitudes of the responses analyzed, whose means ranged from 0.92 to 2.94 pA. (**E**) Many ipRGCs are tuned by depolarization block. (Top) Spike rates at the threshold (I_Φ; Methods) and top ($10^4 \times I_\Phi$) irradiances. "Recov." is the spike rate closest to the threshold rate recovered when irradiance is lowered. (Bottom) Same analysis but for recovery of spike amplitude. Synaptic antagonists, 35°C (A, B, and E) or 23°C (C and D).

to produce the ground state, we measured an action spectrum whose peak wavelength sensitivity (λ_{max}; see Methods) was 467.2 nm. During long-wavelength illumination, the action spectrum had a λ_{max} of 453.5 nm instead, matching the E state of mouse melanopsin (*15*, *16*) and indicating the presence of a second electrically silent state of macaque melanopsin. Statistical analyses indicate that the probability of our observing such widely separated values of λ_{max} by chance is small ($P < 10^{-3}$; Fig. 2D). We also obtained quantitatively similar results in macaque ipRGCs (Fig. 2, E to G, and fig. S5). Thus, our experiments indicate that macaque melanopsin activates from at least two electrically silent states whose preferred wavelengths appear cyan (467.2 nm) and violet (453.5 nm) to trichromatic humans. This spectral separation is roughly half of that between the two cone pigments that define the red-green axis of color vision in humans and macaques (*19*). Under natural light, melanopsin molecules could activate from both silent states (*15*), limiting the cell's wavelength selectivity to promote irradiance encoding.

Because we identified hybrid ipRGCs without immunotagging, our experiments with these cells provide a natural control for effects of the procedure and indicate that it is innocuous for melanopsin function. Following live immunotagging, macaque melanopsin's signaling state retains its thermal stability and its ability to be switched off by long-wavelength light (compare Fig. 1, C to F, with Fig. 2B and fig. S4, A to C), and the silent states retain their distinct spectral sensitivities (compare Fig. 2, C and E, with Fig. 2, F and G and fig. S5B).

Population coding of light intensity by macaque ipRGCs

The intensity of environmental illumination varies over many orders of magnitude (*4*), whereas individual neurons have a much smaller range of distinguishable spike rates. We asked how the intrinsic mechanisms of primate ipRGCs help meet this challenge. We first determined the range over which melanopsin phototransduction drives spikes in these neurons. Rising irradiance caused spiking to increase and then silence for many macaque ipRGCs (11 of 20 cells; Fig. 3, A and B, and fig. S6), giving unimodal tuning curves (intensity-firing relations). For the remainder, spiking increases to a plateau or decreases slightly, giving monotonic tuning curves. Individually, ipRGCs saturated at relatively low firing rates (95% maximal spike rate of 8.2 ± 3.3 Hz; 20 cells) and modulated their spiking over a range of 2.7 ± 0.83 log units of light intensity (19 of 20 cells; 1 excluded because threshold and peak firing rates were similar). Collectively, ipRGCs spanned a range of 5.2 log units, >100 times broader. The most sensitive cells were activated at 1.4 log photons μm^{-2} sec^{-1}, approximately the intensity of moonlight and comparable to the threshold of cone photoreceptors (*20*). The least sensitive were saturated at 6.7 log photons μm^{-2} sec^{-1}, approximately the intensity of full daylight. Comparing half-saturating irradiances, the range is 2.5 log units. Rod and cone inputs are likely to extend this range even further (*3*).

We next asked how some ipRGCs exhibit cone-like sensitivity. High photon capture by ipRGCs would interfere with image vision because ipRGCs lie ahead of rods and cones in the eye's light path. We hypothesized that, as in nocturnal mice (*21*), ipRGC sensitivity in diurnal primates is increased by the properties of the response to each captured photon. This

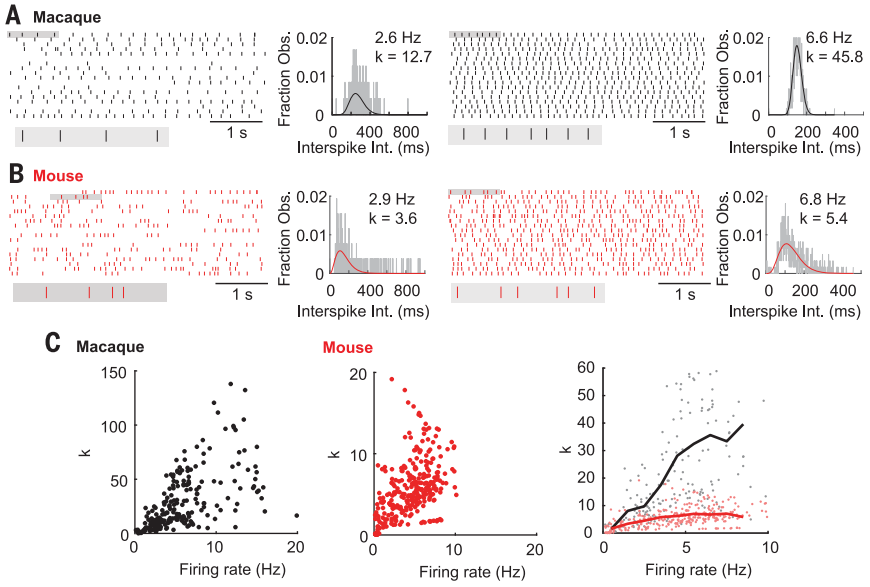

Fig. 4. Regular spiking of macaque ipRGCs. (**A**) Spiking of a macaque ipRGC at low and intermediate firing rates. Insets display shaded portions of spike trains on an expanded time base. Spike times and histograms of interspike intervals (ISIs) are shown. Fits are gamma distributions yielding the regularity parameters (k) indicated. (**B**) The same for a mouse ipRGC. (**C**) Values of k for ISIs in 20 macaque ipRGCs (black) and 26 mouse ipRGCs (red). Each cell is represented by 5 to 16 data points corresponding to stimulus epochs with different firing rates. The correlation of k with firing rate across stimulus epochs for an individual cell was 0.70 ± 0.15 (macaque) or 0.67 ± 0.21 (mouse). Solid lines are averages over 1-Hz bins. For a given firing rate, k has a higher average value in macaque cells than in mouse cells. Saturated (95% maximal) firing rates are similar in both species (see main text). Synaptic antagonists, 35°C.

single photon response originates with one photoactivated melanopsin molecule and is a building block of phototransduction. To define it, we examined the responses to dim flashes. We found linear superposition of small responses (generally <3 pA at room temperature, used for additional recording stability; Fig. 3C, fig. S7; Methods). The variance and mean of linear responses can be used to estimate the amplitude and duration (integration time) of the single photon response (*21*). These parameters were 0.29 ± 0.04 pA and 24 ± 8 s, respectively, when measured at room temperature (Fig. 3D). Extrapolating to body temperature (*21*, *22*) (see Methods), where we measured tuning curves, yields ~0.87 pA and ~11 s. These values exceed those of cone single photon responses, which have an amplitude of ~40 fA and an integration time of ~70 ms (*23*). The large size and long lifetime of the ipRGC single photon response favor sensitivity, the latter by increasing the likelihood that responses to successive photon captures will sum.

Behavioral studies indicate that melanopsin phototransduction is especially critical in bright light (*2*). The subset of monotonically tuned ipRGCs is important in this regime; each unimodally tuned ipRGC is silenced as the light intensity exceeds its preferred range. Unimodal ipRGCs tend to be those that are most sensitive and thus reach their maximum firing rates under relatively low light (intensities at peak firing for unimodal and monotonic ipRGCs are 4.8 ± 0.74 and 6.0 ± 0.62 log photons $\mu m^{-2} s^{-1}$, respectively; $P < 10^{-3}$). Without silencing, these cells would fire at their maximum rates through much of the day. Silencing these relatively uninformative ipRGCs is likely to promote energetic efficiency (*24*). Monotonic ipRGCs are efficient because they fire at their highest rates only in the brightest light, which lasts a comparatively short period of time as the Sun follows its arc.

How does silencing occur? As firing rates fall with increasing irradiance, spikes dwindle in height. This is a signature of depolarization block, where the spike generator is overdriven into a refractory state (Fig. 3, A and E). Depolarization block is increasingly recognized as a physiological state (*25*–*27*), and our data reveal that it tunes primate neurons.

Discussion

In this study, we developed a live immunotagging technique to study a defined subpopulation of macaque neurons. This technique should generalize to other cell types and species. We used it to locate outer-stratifying macaque ipRGCs for functional analysis. Concurrently, we used heterologous expression to study properties of macaque melanopsin in the background of mouse ipRGCs. These approaches revealed specializations at the molecular, cellular, and population scales that allow ipRGCs to encode environmental illumination.

Our results on the outer-stratifying macaque ipRGCs permit comparisons with the orthologous population of outer-stratifying mouse ipRGCs (i.e., M1 ipRGCs) (*15*, *21*, *22*, *26*, *28*). A notable divergence lies in spiking regularity. Interspike intervals (ISIs) in macaque ipRGCs have a coefficient of variation (CV) whose minimum is 0.23 ± 0.09 (20 cells). Fitting ISI distributions with gamma functions (*29*) yields a maximum regularity parameter (k) of 60.8 ± 29.4, more than 3 times higher than the maximum value observed in a survey of macaque cortical neurons (*29*) (Fig. 4, A and C, and fig. S8). Analyzing existing data from mouse ipRGCs (*26*), we find minimum CV and maximum k values of 0.71 ± 0.19 and 8.9 ± 2.6 (26 cells), indicating 3.1 and 6.9 times lower spike regularity than that of macaque ipRGCs, respectively (Fig. 4, B and C, and fig. S8). These differences are not a consequence of different spike rates between macaque and mouse ipRGCs (95% maximal rates of 8.2 ± 3.3 and 7.7 ± 0.9 Hz, respectively; Fig. 4C). In principle, the regular spiking of macaque ipRGCs allows different irradiance levels to be distinguished more readily (fig. S9).

With the exception of regular firing, our study indicates that cell-autonomous mechanisms are largely conserved between mouse and macaque outer-stratifying ipRGCs. Similar to macaque melanopsin, mouse melanopsin has a long-lived signaling state that supports temporal (and hence spatial) integration as well as spectrally distinct silent states that support a degree of chromatic integration (*15*). Similar to macaque ipRGCs, mouse ipRGCs produce a large and prolonged single photon response (*21*, *22*). Mouse ipRGCs also exhibit differential tuning to irradiance (*22*, *26*), resembling macaque ipRGCs in the dynamic ranges of both single cells and the population.

Our findings have the potential to improve artificial lighting, including that used for therapy in mood disorders (*5*). For example, we observe that moderate and not bright light causes the largest number of ipRGCs to signal downstream and that certain wavelengths suppress the persistent activity of these neurons. Future studies should examine how these intrinsic properties combine with rod- and cone-driven signals to shape the outputs of ipRGCs (*2*, *3*, *5*).

Organisms as diverse as coral and humans sense light using melanopsin (*30*). The melanopsin-expressing ipRGCs exist in every mammal so far examined, even subterranean mole rats (*2*). Mice and macaques are separated by ~70 million years of evolution (*31*) as well as by their divergent visual ecologies (e.g., nocturnal versus diurnal). Nonetheless, the functional requirements of irradiance encoding—insensitivity to image detail and the need for

a wide dynamic range—are constant across the divide. The persistence of distinctive molecular, cellular, and population-level features suggests that these functional requirements place strong constraints on neurons that have evolved to report the intensity of environmental illumination.

REFERENCES AND NOTES

1. J. W. Mouland, A. R. Stinchcombe, D. B. Forger, T. M. Brown, R. J. Lucas, *Curr. Biol.* **27**, 1633–1640.e3 (2017).
2. M. T. H. Do, *Neuron* **104**, 205–226 (2019).
3. D. M. Dacey *et al.*, *Nature* **433**, 749–754 (2005).
4. F. Rieke, M. E. Rudd, *Neuron* **64**, 605–616 (2009).
5. R. J. Lucas *et al.*, *Trends Neurosci.* **37**, 1–9 (2014).
6. H.-W. Liao *et al.*, *J. Comp. Neurol.* **524**, 2845–2872 (2016).
7. P. D. Gamlin *et al.*, *Vision Res.* **47**, 946–954 (2007).
8. A. D. Güler *et al.*, *Nature* **453**, 102–105 (2008).
9. M. Hatori *et al.*, *PLOS ONE* **3**, e2451 (2008).
10. A. L. Yarbus, *Eye Movements and Vision* (Plenum Press, 1967).
11. P. Hillman, S. Hochstein, B. Minke, *Physiol. Rev.* **63**, 668–772 (1983).
12. L. S. Mure *et al.*, *PLOS ONE* **4**, e5991 (2009).
13. M. Koyanagi, K. Kubokawa, H. Tsukamoto, Y. Shichida, A. Terakita, *Curr. Biol.* **15**, 1065–1069 (2005).
14. J. Zylberberg, B. W. Strowbridge, *Annu. Rev. Neurosci.* **40**, 603–627 (2017).
15. A. J. Emanuel, M. T. H. Do, *Neuron* **85**, 1043–1055 (2015).
16. T. Matsuyama, T. Yamashita, Y. Imamoto, Y. Shichida, *Biochemistry* **51**, 5454–5462 (2012).
17. J. L. Ecker *et al.*, *Neuron* **67**, 49–60 (2010).
18. V. I. Govardovskii, N. Fyhrquist, T. Reuter, D. G. Kuzmin, K. Donner, *Vis. Neurosci.* **17**, 509–528 (2000).
19. S. L. Merbs, J. Nathans, *Nature* **356**, 433–435 (1992).
20. N. T. Ingram, A. P. Sampath, G. L. Fain, *J. Physiol.* **594**, 5415–5426 (2016).
21. M. T. H. Do *et al.*, *Nature* **457**, 281–287 (2009).
22. A. J. Emanuel, K. Kapur, M. T. H. Do, *Cell Rep.* **21**, 1048–1062 (2017).
23. L. H. Cao, D. G. Luo, K. W. Yau, *Proc. Natl. Acad. Sci. U.S.A.* **111**, 2752–2757 (2014).
24. P. Sterling, S. Laughlin, *Principles of Neural Design* (MIT Press, 2015).
25. M. D. Belle, C. O. Diekman, D. B. Forger, H. D. Piggins, *Science* **326**, 281–284 (2009).
26. E. S. Milner, M. T. H. Do, *Cell* **171**, 865–876.e16 (2017).
27. S. Wienbar, G. W. Schwartz, *Neuron* **110**, 2110–2123.e4 (2022).
28. M. T. H. Do, K.-W. Yau, *Proc. Natl. Acad. Sci. U.S.A.* **110**, 7470–7475 (2013).
29. G. Maimon, J. A. Assad, *Neuron* **62**, 426–440 (2009).
30. M. T. H. Do, K.-W. Yau, *Physiol. Rev.* **90**, 1547–1581 (2010).
31. T. R. Disotell, A. J. Tosi, *Genome Biol.* **8**, 226 (2007).

ACKNOWLEDGMENTS

We thank those who shared materials: J. Assad, R. Born, C. Cetrulo, J. DiCarlo, A. Hall, R. P. Johnson, M. Livingstone, J. Madsen, T. Moore, M. Nedelman, M. Papisov, D. Rosene, and S. Smith. We thank R. Born and M. Greenberg for helping to initiate and sustain this research program; V. Berezovskii, E. Cosgrove, E. Curran, E. Egan, and R. Adams for logistical and technical assistance; C. Wang, Y. Zhang, and Z. He for viral vectors; F. Rieke and R. Sinha for expertise on the primate retina; C. Cepko and W. Xiong for expertise on molecular biology; D. Vavvas for microsurgical techniques; S. Hattar for the Opn4^{Cre} mouse line; D. Felis, W. Lorenzen, and J. Wu for institutional infrastructure; and F. Caval-Holme for comments on the manuscript. M. T. H. Do is affiliated with the Center for Brain Science of Harvard University, the Division of Sleep Medicine of Harvard Medical School, and the Broad Institute of MIT and Harvard. **Funding:** This work was supported by the following: National Institutes of Health R01EY023648, R01EY030628, R01EY034089, and R21EY025840 (to M.T.H.D.); R01EY025555 (to P.D.G. and M.T.H.D.); R21EY028633 (to J.R.S. and M.T.H.D.); F31EY025466 (to E.S.M.); P50HD105351 (to Boston Children's Hospital IDDRC); P30EY012196 (to Harvard Medical School); The National Science Foundation (GFRP to G.S.B. and A.J.E.); The BrightFocus Foundation M2014055 (to M.T.H.D.); the Lefler Center (to A.L. and P.M.); the Neurobiology Department of Harvard Medical School (to A.L.); the Tommy Fuss Center (to P.M.). **Author contributions:** A.L., G.S.B., A.J.E., and M.T.H.D. developed the method of live immunotagging in retina. A.L., G.S.B., and M.T.H.D. developed methods of obtaining, transporting, and maintaining live tissue. A.L., G.S.B., M.C.B., A.J.E., and M.T.H.D. procured tissue. A.L. obtained perforated-patch electrophysiological data except for those in fig. S4, A to C, obtained by N.-M.V. E.S.M. obtained all loose-patch electrophysiological data except for one cell, contributed by P.M., A.L., E.S.M., and M.T.H.D. analyzed electrophysiological data. Y.-R.P. cloned and subcloned macaque melanopsin in the laboratory of J.R.S.-P.D.G., and M.T.H.D. generated and validated custom antibodies. E.S.M. and H.A.B. performed intraocular injections. M.C.B. and M.T.H.D. conducted immunohistochemical experiments on fixed tissues. A.L. and M.T.H.D. wrote the manuscript with input from all authors. M.T.H.D. conceived of live immunotagging and of exchanging melanopsin species within native neurons. H.A.B., M.C.B., G.S.B., A.J.E., P.M., and N.-M.V. are listed alphabetically. **Competing interests:** The authors declare no competing interests. **Data and materials availability:** Materials are available upon request to michael.do@childrens.harvard.edu. Data are stored and curated by Harvard Dataverse (*41*).

SUPPLEMENTARY MATERIALS

science.org/doi/10.1126/science.ade2024
Materials and Methods
Figs. S1 to S9
References (*32*–*41*)
MDAR Reproducibility Checklist

View/request a protocol for this paper from *Bio-protocol*.

Submitted 2 August 2022; accepted 21 November 2022
10.1126/science.ade2024